Global observations of the land breeze

Sarah T. Gille

Scripps Institution of Oceanography and Department of Mechanical and Aerospace Engineering, University of California, San Diego, California, USA

Stefan G. Llewellyn Smith and Nicholas M. Statom

Department of Mechanical and Aerospace Engineering, University of California, San Diego, California, USA

Received 2 December 2004; revised 7 January 2005; accepted 9 February 2005; published 4 March 2005.

[1] Four-times daily satellite wind observations from the QuikSCAT and ADEOS-II tandem scatterometer mission are used to study the land/sea breeze circulation. These observations provide a global view of diurnal wind variations over the ocean. Results agree with frictional linear theory: winds follow an elliptical hodograph through the course of the day, but indicate that diurnal wind variations propagate offshore progressively like nonlinear gravity waves and are detectable several hundred kilometers from the coast. **Citation:** Gille, S. T., S. G. Llewellyn Smith, and N. M. Statom (2005), Global observations of the land breeze, *Geophys. Res. Lett.*, *32*, L05605, doi:10.1029/2004GL022139.

1. Introduction

[2] In coastal regions, the land surface warms and cools more rapidly than the ocean in response to daytime solar heating. The resulting diurnal cycle in air-sea temperature difference drives an onshore wind during the day and an offshore wind at night. These wind patterns, known as the sea breeze and land breeze respectively, have important implications for coastal meteorology, for air quality and pollutant dispersal in densely populated coastal regions [*Miller et al.*, 2003], and for climate processes influenced by diurnal forcing, such as ocean mixed-layer heat storage.

[3] Past observational studies of the land and sea breeze have focused on describing diurnal variations in limited regions where in situ meteorological data were available [*Dorman*, 1982; *Alpert et al.*, 1984; *Simpson*, 1994; *Lerczak et al.*, 2001; *Miller et al.*, 2003; *Wichink Kruit et al.*, 2004]. Because in situ observations have limited geographic range, these studies identified processes that depend on orography or other local conditions, and could not distinguish local variations from global variations. Here we use scatterometer winds from the SeaWinds instruments aboard the QuikSCAT and ADEOS-II satellites to study the diurnal evolution of the wind over the global ocean.

2. Data and Methods

[4] SeaWinds scatterometers were launched in 1999 aboard the QuikSCAT satellite and in 2002 aboard ADEOS-II. The instruments were designed to measure winds with an accuracy of 2 m s^{-1} in speed and 20° in direction, with wind observations reported in 25 km pixels along a grid centered along the satellite ground track [*Lungu*, 2001, 2002]. QuikSCAT and ADEOS-II functioned as a tandem mission between April and October 2003, providing a total of 198 days of data before ADEOS-II's premature failure. Both satellites followed sun synchronous orbits, with QuikSCAT observing at roughly 6:00 and 18:00 local time and ADEOS-II observing at roughly 10:30 and 22:30 local time.

[5] Earlier analyses based on QuikSCAT observations alone have shown that morning and evening wind observations are statistically different along most coastlines of the world and throughout the tropical ocean [*Gille et al.*, 2003; *Perlin et al.*, 2004]. The addition of ADEOS-II observations allows us to examine the details of the diurnal variability.

[6] For this analysis, all rain-free scatterometer wind measurements collected during the six-month tandem mission were sorted geographically into 0.25° latitude by 0.25° longitude bins, temporally into one of four time bins centered at approximately 6:00, 10:30, 18:00, or 22:30. Winds were averaged to produce mean zonal (u) and meridional (v) components in each bin. Because of the Earth's rotation relative to the satellite orbit, the mean time of local observations differs by up to 68 minutes from the mean observation time at the equator, and hence an average measurement time was computed for each spatio-temporal bin.

[7] In situ measurements have typically found near-elliptical variability [*Haurwitz*, 1947; *Schmidt*, 1947; *Alpert et al.*, 1984]. Therefore binned components were least-squares fitted as follows:

$$u = u_0 + u_1 \cos \omega t + u_2 \sin \omega t, \tag{1}$$

$$v = v_0 + v_1 \cos \omega t + v_2 \sin \omega t, \tag{2}$$

where $\omega = 2\pi$ day^{-1}. The least-squares fit is slightly overdetermined, with 8 quantities used to determine six parameters. The least-squares fits of u_1, u_2, v_1 and v_2 were used to represent the wind observations in an elliptical hodograph.

[8] Winds align with the major axis of the ellipse at time:

$$\omega t = \frac{1}{2} \operatorname{atan}\left[\frac{2(u_1 u_2 + v_1 v_2)}{u_1^2 + v_1^2 - u_2^2 - v_2^2}\right]. \tag{3}$$

The semi-major axis has length

$$a = \sqrt{(u_1 \cos \omega t + u_2 \sin \omega t)^2 + (v_1 \cos \omega t + v_2 \sin \omega t)^2}, \tag{4}$$

0094-8276/05/2004GL022139

and corresponds to the direction of maximum diurnal variation. The semi-minor axis has length

$$b = \sqrt{(-u_1 \sin \omega t + u_2 \cos \omega t)^2 + (-v_1 \sin \omega t + v_2 \cos \omega t)^2}, \quad (5)$$

and is oriented along the direction of minimum variation, orthogonal to a. The ellipse tilts relative to parallels of latitude by an angle:

$$\phi = \text{atan}\left[\frac{v_1 \cos \omega t + v_2 \sin \omega t}{u_1 \cos \omega t + u_2 \sin \omega t}\right]. \quad (6)$$

3. Land Breeze Characteristics

[9] Figure 1a shows a global map of a where it exceeds 3 times its estimated standard error and a selection of wind ellipses. Because the parameters that define the wind ellipse are calculated through a set of non-linear equations, error bars were estimated using a Monte Carlo procedure. One hundred realizations of random data were created by adding to the observations normally distributed perturbations with a standard deviation equal to the standard error in the observations. On average, for locations with a statistically significant land breeze, the diurnal cycle accounts for 17% of the wind variability resolved by the tandem mission, and 92% of this resolved diurnal variability is explained by the elliptical fit. Although sea surface temperature and atmospheric stability influence scatterometer retrievals, these effects are expected to be small compared with the diurnal signals seen here.

[10] In Figure 1a, a strong diurnal cycle is visible across the entire Pacific and Atlantic Oceans equatorward of 30° latitude and along coastlines at all latitudes. (Diurnal variations are not statistically significant in the tropical Indian Ocean, because of the high variance associated with the monsoon.) The amplitude of the wind is strongest in pixels closest to the coast and attenuates with distance from the shore, as predicted by theory [*Walsh*, 1974; *Niino*, 1987]. Poleward of 30° latitude, statistically significant diurnal cycles are more evident along Northern Hemisphere coastlines than along South American coastlines. This is expected, because the land breeze is strongest in summer [*Gille et al.*, 2003], and ADEOS-II operated only in boreal summer.

[11] The offshore extent of the land breeze is shown as a function of latitude in Figure 2a. The maximum extent in each 1° latitude bin was determined by finding the first 25 km interval from the shore in which no statistically significant land breeze was observed at any longitude. The results, though not strongly sensitive to bin width, may underestimate offshore extent, particularly if the variance of the winds increases with distance from the coast. The land breeze is detectable up to 300 km offshore at 30° latitude, and up to 100 km offshore poleward of 40° latitude. Equatorward of 30°, the north-south orientation of the wind ellipses in the central Pacific and Atlantic Oceans implies that diurnal variations are controlled by local convective processes that enhance the Hadley cell [*Dai and Deser*, 1999] rather than daytime heating of distant land masses. Nonetheless, in the tropics, the influence of land appears to extend several hundred kilometers from shore and consistently exceeds the onshore extent of the sea breeze, which has been reported to be between 15 km on the Beaufort Sea coast in Alaska [*Kozo*, 1982] and 200 km in northern Australia [*Simpson*, 1994; *Miller et al.*, 2003]. The offshore extent of the land breeze is not as far as implied by inviscid linear theory, which predicts infinite propagation equatorward of 30° latitude [*Rotunno*, 1983], but it is further than implied by frictional linear theory, which predicts a gradual change in offshore extent between high and low latitudes [*Niino*, 1987] (see Figure 2a).

[12] In coastal regions, wind ellipses are expected to be roughly perpendicular to the coastline, with the exact orientation predicted to depend on several factors including latitude and friction [*Schmidt*, 1947; *Alpert et al.*, 1984]. Figure 2b shows that on average the angular orientation of the major axis relative to a normal to the coastline varies linearly with latitude. Angular orientation was computed in 1° latitude bins for all statistically significant sea breeze locations within 3° of the coast. Since wind data are spatially correlated, standard errors were estimated by dividing the standard deviation by $\sqrt{N/16}$, where N is the number of quarter degree bins available, i.e. by assuming that data decorrelate over 1° length scales in coastal regions. Also shown in Figure 2b are theoretical predictions by *Alpert et al.* [1984], who obtained a near-linear dependence with latitude. Our study provides global verification of this prediction and shows that the best fit is obtained when the linear drag term k has magnitude roughly equal to the angular rotation rate of the Earth ω.

[13] Latitude also affects the wind ellipse eccentricity, $e \equiv \sqrt{a^2 - b^2}/a$. The eccentricity exceeds 0.5 everywhere and is almost always greater than 0.9. Hence the dominant wind motion is a pattern of alternating onshore and offshore flow. Scatterometer eccentricities, shown in Figure 2c, were computed for the same bins as angular orientations. Average eccentricities roughly match Alpert et al.'s predictions of high eccentricity near the equator, a minimum at mid-latitudes, and higher eccentricity at the poles.

[14] Because of the Coriolis effect, the ellipse's direction of rotation is expected to be anticyclonic (i.e. clockwise in the Northern Hemisphere). We find that the direction of rotation is consistent with this expectation (see Figure 1b). Regional observations of the sea breeze have often reported winds rotating in the opposite direction [e.g., *Alpert et al.*, 1984]. Our analysis indicates that on a global scale cyclonic rotation is unusual and is therefore probably linked to the details of regional meteorology and orography. Along the equator where the Coriolis force is zero, both clockwise and counterclockwise rotation occur.

[15] Figure 1c shows a global map of the observed time of day when winds reach their maximum strength. Maximum air-sea temperature differences are typically thought to occur around 2 pm [*Haurwitz*, 1947]. Figure 1c indicates the maximum land breeze occurs between 4 pm and 8 pm at scatterometer measurements closest to the coast. With increasing distance from the coast, the time of day when the maximum wind occurs becomes progressively later, so that several hundred kilometers offshore, the maximum wind speed occurs around 10 pm. Exceptions occur near major topographic features such as the Andes and the Namibian highlands and along the east coast of Africa,

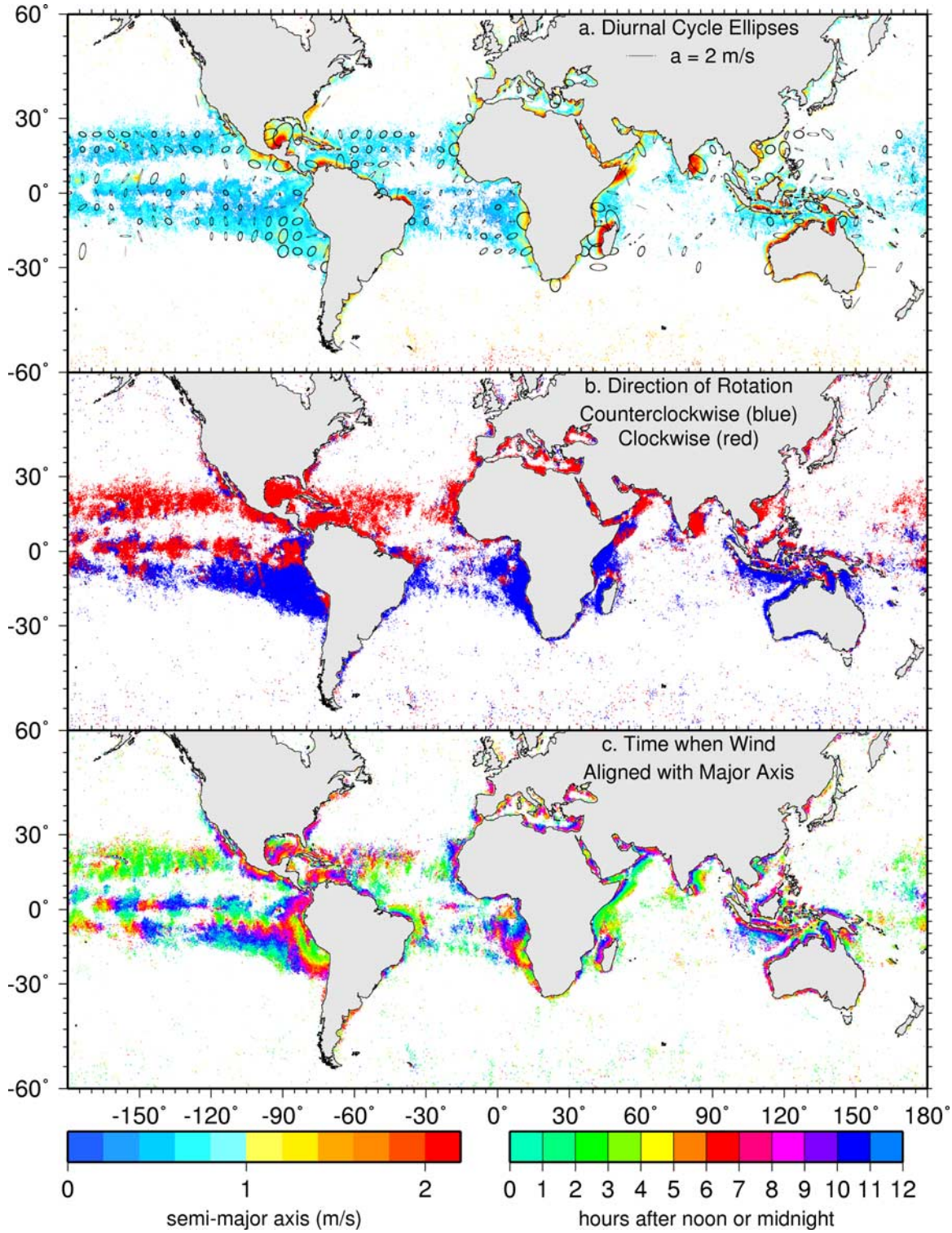

Figure 1. (a) Strength of diurnal wind cycle, with major axis plotted in color in locations where it is statistically significant, and wind ellipses plotted every 6° in locations that are either within 10° of land or equatorward of 30° latitude. Reference line indicates the major axis for an ellipse with semi-major axis $a = 2$ m s^{-1}. (b) Direction of rotation of wind. Red indicates clockwise and blue counter-clockwise rotation. (c) Time of day when wind is aligned with major axis. (Winds are aligned with the major axis twice a day.)

where the nearshore maximum may occur after the offshore maximum.

[16] Finally, from the phase information shown in Figure 1c, average offshore propagation rates, i.e. the velocity of the land breeze front, were computed in 1° latitudinal bins. Overall there is no clear latitudinal trend. At high latitudes, few data are available and outliers are common. Equatorward of 30°, propagation rates varied

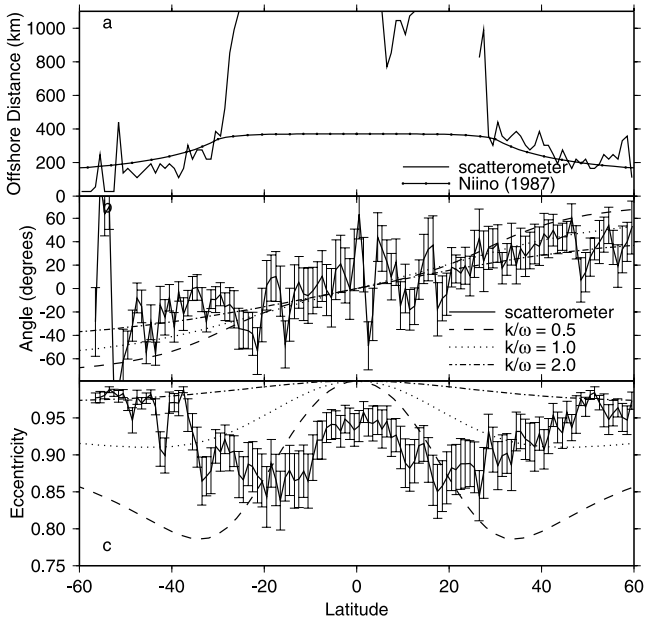

Figure 2. (a) Maximum offshore extent of the land breeze as a function of latitude and predictions from Niino's linear theory [*Niino*, 1987] arbitrarily scaled to match observed offshore extents poleward of 30°. (b) Angular orientation of the wind ellipse relative to a normal to the coastline and predictions from *Alpert et al.* [1984] which uses a linear drag k that is scaled relative to the rotation rate ω. Positive angles represent a rotation to the right of the normal. (c) Eccentricity of wind ellipses, again shown with predictions from *Alpert et al.* [1984].

between 2 and 15 m s^{-1}, with one outlier of 29 m s^{-1}, implying an average propagation of 9 m s^{-1}, with standard deviation 4 m s^{-1}.

[17] These propagation rates are roughly an order of magnitude greater than the major axis amplitudes. They also exceed the component of mean flow perpendicular to the coast, which averages 0.6 m s^{-1} with standard deviation 2.9 m s^{-1} for locations within 550 km of the coast and equatorward of 30° that have a statistically significant diurnal cycle. Theory and laboratory experiments predict that the land breeze front should behave as a gravity current with velocity $U = \kappa\sqrt{g'd}$, where κ is a constant, $g' = g\Delta T/T$ is reduced gravity, and d is a scale height. In contrast with the linear theories used to predict eccentricity and angular orientation of the tidal ellipses, gravity currents depend crucially on nonlinear processes. For typical values κ = 0.62 [*Simpson*, 1969], T = 300 K, ΔT = 5 K, and d = 1000 m, U is 8 m s^{-1}, in rough agreement with our observations.

4. Summary

[18] This study describes the high-resolution structure of diurnal variability in winds, providing global spatio-temporal observations of the land breeze. Simple linear theory [*Alpert et al.*, 1984], with appropriately chosen drag parameters, explains the orientation, eccentricity, and direction of rotation of the wind hodographs. Scalings derived from laboratory gravity current experiments are able to predict the propagation speed of the land breeze. The significant offshore extent of the land breeze system over the ocean has important implications for our understanding of pollutant dispersal. Coastal pollutants will be transported with the advective velocity of the land breeze front, i.e. the gravity current speed, and will hence propagate out to sea fast and far. The results shown here are also important for upper ocean coastal mixed-layer dynamics, because they show that the land's influence is felt far from shore. Since land breeze wind forcing and solar heating are in phase, this may influence global upper ocean heat storage and gas exchange processes.

[19] **Acknowledgment.** This work was supported by the NASA Ocean Vector Wind Science Team, JPL contract 1222984.

References

Alpert, P., M. Kusuda, and N. Abe (1984), Anticlockwise rotation, eccentricity and tilt angle of the wind hodograph. Part II: An observational study, *J. Atmos. Sci.*, *41*, 3568–3583.

Dai, A., and C. Deser (1999), Diurnal and semidiurnal variations in global surface wind divergence fields, *J. Geophys. Res.*, *104*, 31,109–31,125.

Dorman, C. E. (1982), Winds between San Diego and San Clemente Island, *J. Geophys. Res.*, *87*, 9636–9646.

Gille, S. T., S. G. Llewellyn Smith, and S. M. Lee (2003), Measuring the sea breeze from QuikSCAT scatterometry, *Geophys. Res. Lett.*, *30*(3), 1114, doi:10.1029/2002GL016230.

Haurwitz, B. (1947), Comments on the sea-breeze circulation, *J. Meteorol.*, *4*, 1–8.

Kozo, T. L. (1982), An observational study of sea breezes along the Alaskan Beaufort sea coast, *J. Appl. Meteorol.*, *21*, 891–905.

Lerczak, J. A., M. C. Hendershott, and C. D. Winant (2001), Observations and modeling of coastal internal waves driven by a diurnal sea breeze, *J. Geophys. Res.*, *106*, 19,715–19,729.

Lungu, T. (2001), QuikSCAT science data product user's manual, overview and geophysical data products, version 2.2, *JPL Doc. D-18053*, 95 pp., Jet Propul. Lab., Pasadena, Calif.

Lungu, T. (2002), Seawinds science data product user's manual, version 1.0, *JPL Doc. D-21551*, 128 pp., Jet Propul. Lab., Pasadena, Calif.

Miller, S. T. K., B. D. Keim, R. W. Talbot, and H. Mao (2003), Sea breeze: Structure, forecasting, and impacts, *Rev. Geophys.*, *41*(3), 1011, doi:10.1029/2003RG000124.

Niino, H. (1987), The linear theory of land and sea breeze circulation, *J. Meteorol. Soc. Jpn.*, *65*, 901–921.

Perlin, N., R. M. Samelson, and D. B. Chelton (2004), Scatterometer and model wind and wind stress in the Oregon–Northern California coastal zone, *Mon. Weather Rev.*, *132*, 2110–2129.

Rotunno, R. (1983), On the linear theory of the land and sea breeze, *J. Atmos. Sci.*, *40*, 1999–2009.

Schmidt, F. H. (1947), An elementary theory of the land- and sea-breeze circulation, *J. Meteorol.*, *4*, 9–15.

Simpson, J. E. (1969), A comparison between laboratory currents and atmospheric density currents, *Q. J. R. Meteorol. Soc.*, *95*, 758–765.

Simpson, J. E. (1994), *Sea Breeze and Local Wind*, Cambridge Univ. Press, New York.

Walsh, J. E. (1974), Sea breeze theory and applications, *J. Atmos. Sci.*, *31*, 2012–2026.

Wichink Kruit, R. J., A. A. M. Holtslag, and A. B. C. Tijm (2004), Scaling of the sea-breeze strength with observations in the Netherlands, *Boundary Layer Meteorol.*, *112*, 369–380.

S. T. Gille, Scripps Institution of Oceanography, University of California, La Jolla, CA 92093-0230, USA. (sgille@ucsd.edu)

S. G. Llewellyn Smith and N. M. Statom, Department of Mechanical and Aerospace Engineering, University of California, San Diego, CA 92093-0411, USA.